Soft matter dynamics: Accelerated fluid squeeze-out during slip

W. Hutt (iD), and B. N. J. Persson

View Online   Export Citation   CrossMark

ARTICLES YOU MAY BE INTERESTED IN

AIP Publishing

Soft matter dynamics: Accelerated fluid squeeze-out during slip

W. Hutt[1] and B. N. J. Persson[2,a)]
[1]*Pfisterer Kontaktsysteme GmbH, Rosenstraße 44, 73650 Winterbach, Germany*
[2]*PGI-1, FZ Jülich, Germany*

Using a Leonardo da Vinci experimental setup (constant driving force), we study the dependency of lubricated rubber friction on the time of stationary contact and on the sliding distance. We slide rectangular rubber blocks on smooth polymer surfaces lubricated by glycerol or by a grease. We observe a remarkable effect: during stationary contact the lubricant is only very slowly removed from the rubber-polymer interface, while during slip it is very rapidly removed resulting (for the grease lubricated surface) in complete stop of motion after a short time period, corresponding to a slip distance typically of order only a few times the length of the rubber block in the sliding direction. For an elastically stiff material, poly(methyl methacrylate), we observe the opposite effect: the sliding speed increases with time (acceleration), and the lubricant film thickness appears to increase. We propose an explanation for the observed effect based on transient elastohydrodynamics, which may be relevant also for other soft contacts. © *2016 AIP Publishing LLC.* [http://dx.doi.org/10.1063/1.4944384]

I. INTRODUCTION

The nature of the lubricated contact between soft elastic bodies is one of the central topics in tribology, with applications to the human joints and eyes,[1] dynamic rubber seals, and the tire-road interaction, to name just a few examples. However, these problems are also very complex involving large elastic deformations and fluid flow between narrowly spaced walls and in irregular channels.[2] For smooth spherical and cylindrical bodies in steady sliding on flat lubricated substrates (i.e., without surface roughness), such *elastohydrodynamic* problems are now well understood.[3,4] However, for more realistic cases involving non-steady sliding, with surfaces with roughness on many length scales, and with non-Newtonian fluids, rather little is known.[5]

For lubricated contacts, the force necessary to start sliding, the so-called breakloose friction force, depends on the time of stationary contact. During stationary contact, the lubricant fluid is continuously squeezed out from the asperity contact regions, resulting in a solid contact area, and a breakloose friction force, which increases monotonically with the time of contact. This problem has been studied experimentally in detail in several publications,[6,7] and very puzzling observations have been made, e.g., in Ref. 7, the breakloose friction force was found to be very similar for high and low viscosity fluids, and it increased faster with the contact time than expected from theoretical argument. In this paper, we will report on another surprising experimental results and propose an explanation which may also be relevant to the problem mentioned above.

In this study, we slide rectangular silicone rubber (powersil 600 A/B), tread rubber, and poly(methyl methacrylate) (PMMA) blocks on smooth polymer surfaces lubricated by glycerol or by a grease. Glycerol is a Newtonian fluid (the shear stress is proportional to the shear rate), while the grease

is a viscoplastic material which behaves as a rigid body at very low stresses but flows as a viscous (shear thinning) fluid at high stress. For the rubber blocks with the (for the relevant low frequencies) Young's modulus $E \approx 1$ MPa (silicon rubber) and $E \approx 10$ MPa (tread rubber), we observe a surprising result: during stationary contact, the lubricant is only very slowly removed from the rubber-polymer interface, while during slip, it is very rapidly removed and the motion stops after a short sliding distance. For PMMA, which is a glassy polymer with a Young's elastic modulus of order a few GPa, we observe the opposite effect: during slip, the sliding speed increases with time (acceleration). We propose an explanation for the observed effect based on transient elastohydrodynamics, which may be relevant also for other soft lubricated contacts.

II. EXPERIMENTAL SETUP

The measured data presented below were obtained using the Leonardo da Vinci setup shown in Fig. 1. The slider consists of two rubber (or PMMA) blocks glued to a wood plate. One block is at the front of the wood plate and the other at the end of the wood plate. The blocks are 5 mm thick, $L_y = 4$ cm long orthogonal to the sliding direction, and $L_x = 1.25$ cm long in the sliding direction, giving the total nominal contact area $A_0 = 2 L_x L_y = 10$ cm^2. The normal force is generated by adding lead blocks (total mass M) on top of the wood plate, up to $M \approx 30$ kg. Similarly the driving force is generated by adding small (0.25 kg) lead blocks in the container M' in Fig. 1. The substrate is a red colored polymer (an epoxy resin with silica particle filler) with a very smooth surface lubricated by a grease or by glycerol. The sliding distance as a function of time is measured using a distance sensor. This simple friction tester can be used for obtaining the friction coefficient $\mu = M'/M$ as a function of sliding velocity.[8] Here we are
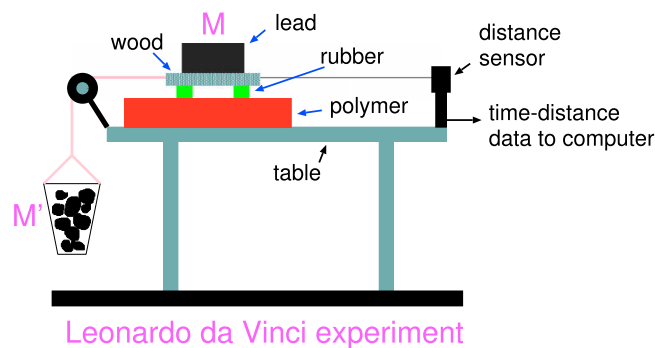
a)www.MultiscaleConsulting.com

FIG. 1. Simple friction tester (schematic) used for obtaining the friction coefficient $\mu = M'/M$ as a function of the sliding speed. The sliding distance is measured using a rope-pull-out distance sensor.

instead interested in non-steady sliding for different driving forces $F_x = M'g = \mu F_N$, where the normal force $F_N = Mg$.

The grease we use is a perfluorinated polyether oil with a polytetraflouroethylene (PTFE) thickener (Klüber lubrication) with the room temperature viscosity $\eta \approx 10$ Pa s at the shear rate $\dot{\gamma} \approx 10^3$ s^{-1}, and a yield stress of order 10^3 Pa. The glycerol at the temperature of our measurements has the viscosity $\eta \approx 2$ Pa s. For more information about surface topography and material properties, see Appendix A.

III. EXPERIMENTAL RESULTS AND INTERPRETATION

Fig. 2 shows the sliding distance as a function of time for the soft silicon rubber (red line), the tread rubber (green line), and for PMMA (blue line). The substrate surface is lubricated by the grease. The nominal contact pressure $p = F_N/A_0 = 0.09$ MPa. In all cases, the driving force $F_x = \mu F_N$ is abruptly increased from zero to μF_N with $\mu \approx 0.16$. For the two types of rubber, the motion stops after similar time periods, but the stiffer tread rubber slides much longer distance before stop. For the PMMA the velocity increases monotonically with time (accelerated motion).

Fig. 3(a) shows a picture of the sliding track after the silicon rubber block (initial position given by the dashed
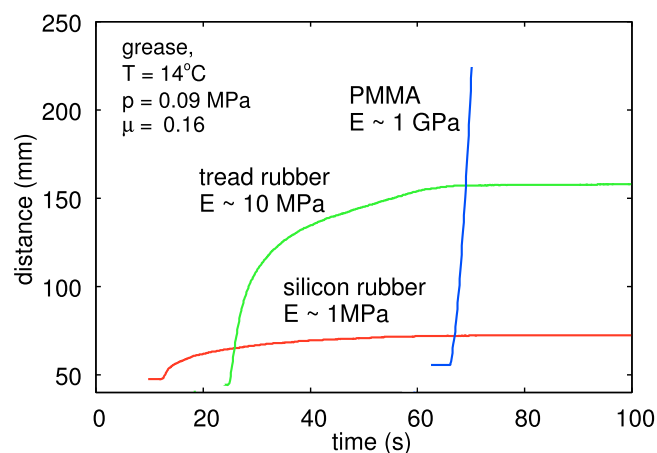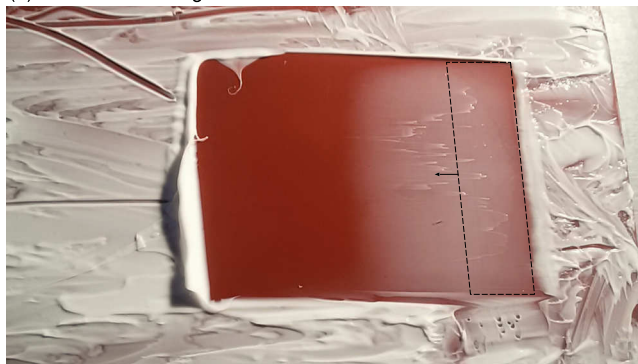

FIG. 2. The sliding distance as a function of time for soft silicon rubber (red line), a tread rubber (green line), and for PMMA (blue line), sliding on a polymer surface lubricated by a grease.
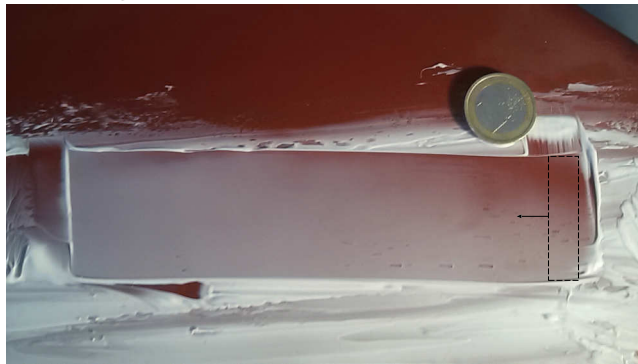

(a) silicone rubber - grease

(b) PMMA - grease

FIG. 3. (a) Picture of the sliding track after a rectangular rubber block (initial position given by the dashed rectangle) is slid on the grease (white color paste) lubricated polymer (red) surface. (b) Picture of the sliding track after a rectangular PMMA block (with the same size as the rubber blocks) is slid on the same grease lubricated surface.

rectangle) is slid on the grease (white colored paste) lubricated polymer (red) surface. The result is after a similar slip event as in Fig. 2 but with $\mu = 0.45$. Note that it appears as if the grease is continuously removed during the sliding action, and to the naked eye the contact area appears dry (or clean) at the end of the sliding. However, as will be shown below, in reality a thin grease film still exists on the surfaces.

Fig. 3(b) shows the sliding track after the PMMA block is slid on the same surface as in Fig. 3(a). In this case, the block accelerates (until the motion comes to a stop when the driving mass M' hit the floor), and it appears as if the grease film thickness increases with the sliding distance.[9]

We now propose an explanation for the surprising results presented in Figs. 2 and 3. When a rigid body with a flat surface is squeezed against a flat rigid countersurface in a fluid, because of the fluid viscosity a pressure will develop in the fluid, which is maximal in the center of the contact region (see, e.g., Refs. 10 and 11). For elastic solids (Young's modulus E), the fluid pressure will deform the solid such that the separation between the solids will have a maximum at the center of the contact region, see Fig. 4(a). This deformations of the bottom surface of the block increases when the elastic modulus of the solids decreases, and the surface slope at any point on the rubber surface will scale as $du/dx \sim p/E$ where p is the nominal contact pressure. With the nominal contact pressures used in this study, the effect is large for the rubber materials but negligible for the PMMA.
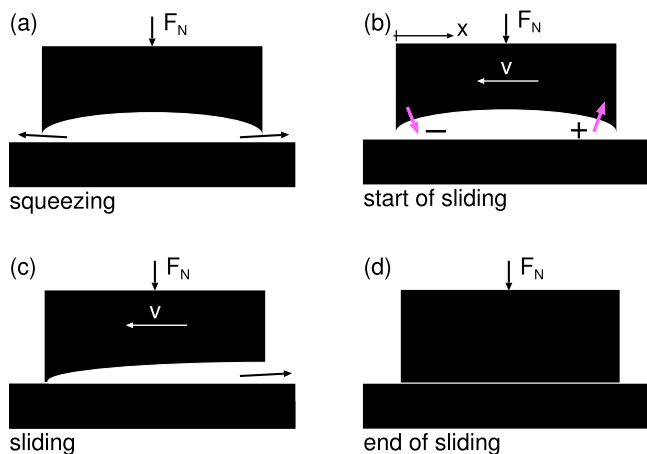
FIG. 4. Proposed explanation for fluid removal during slip. During squeezing, the bottom surface of the rubber block deforms as in (a). During sliding, the surface separation changes as indicated in (b)–(d).
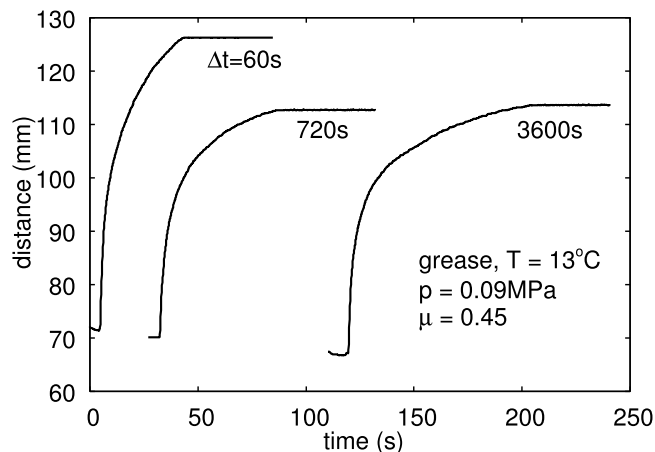

FIG. 5. Sliding dynamics for the interface lubricated by a grease. The sliding distance is shown as a function of the time, after three different times Δt of stationary contact.

If we now start to slide, the fluid pressure will decrease at the inlet side because of the increasing surface separation with increasing x, while it will increase on the exit side due to the decreasing surface separation with increasing x. Thus, on the rubber surface will act a fluid pressure which will deform the rubber as indicated by the pink arrows in (b). Hence, during sliding, the surfaces will be deformed as in (c), which will strongly reduce the inflow of fluid at the inlet side, and make it easy for fluid to disappear on the exit side. As a result the separation between the surfaces will rapidly decrease, and at the stop of sliding, the surface separation may be as in (d). This explains why for the silicon rubber block, sliding just ∼3 times the width of the block in the sliding direction results in a nearly dry contact area. We will refer to the process above as the dynamic scrape mechanism.

Here we point out that assuming that dewetting does not occur (see Appendix B), squeeze-out calculations (no sliding) predict very long squeeze-out time: Consider the fluid squeeze-out between a rectangular rubber block and the substrate. We assume the length L_x of the rubber block in the sliding direction (x-direction) is much smaller than the width of the rubber block in the orthogonal y-direction. In that case, if both surfaces are perfectly smooth, the thickness $h(t)$ of the fluid layer at time t is given by (see, e.g., Refs. 10 and 11)

$$\frac{1}{h^2(t)} - \frac{1}{h^2(0)} = \frac{2tp_0}{\eta L_x^2},$$

or when $h(0)/h(t) \gg 1$,

$$t = \frac{\eta}{2p_0}\left(\frac{L_x}{h}\right)^2. \tag{1}$$

Thus for glycerol with the viscosity 2 Pa s, and assuming the squeezing pressure $p_0 = 0.1$ MPa and $L_x = 1$ cm, we obtain from (1) that it takes $t \approx 10^9$ s (or 30 yr) to squeeze-out the fluid until the separation $h \approx 1$ nm. For an elastic block, the squeeze-out time is even longer because of the upward bending of the surface at the center of the contact area. When the surface roughness is included in the analysis, the squeeze-out is faster, $t \approx 10^6$ s (or about 10 days) (see Appendix B). For the grease, which has a much higher effective viscosity than glycerol

(unless the shear rate is very high), the squeeze-out time would be even longer. Clearly, the sliding action enormously speeds up the removal of the lubricant fluid from the contact interface.

We now present more experimental results to illustrate other aspects of the sliding dynamics. Figs. 5 and 6 show results for the interface lubricated by the grease. In Fig. 5, the sliding distance is shown as a function of time t, after three different times Δt of stationary contact. Thus after applying the normal load $F_N = pA_0$ (with $p = 0.09$ MPa), we waited the time Δt before applying the driving force. Note that the sliding motion stops after some time. For the interface lubricated by glycerol, we do not observe the same effect (see below), and we therefore attribute it to the finite yield stress of the grease. The squeeze-out (or waiting) time Δt has no big influence on the sliding distance, but when Δt increases, the sliding time (i.e., the time it takes for the slider to stop to move) increases. We attribute this to squeeze-out during the time of stationary contact, which reduces the film thickness and increases the viscous friction and hence reduce the sliding speed.

Fig. 6 shows results when the driving force is increased in steps. At time $t = 0$, the driving force is increased from zero to
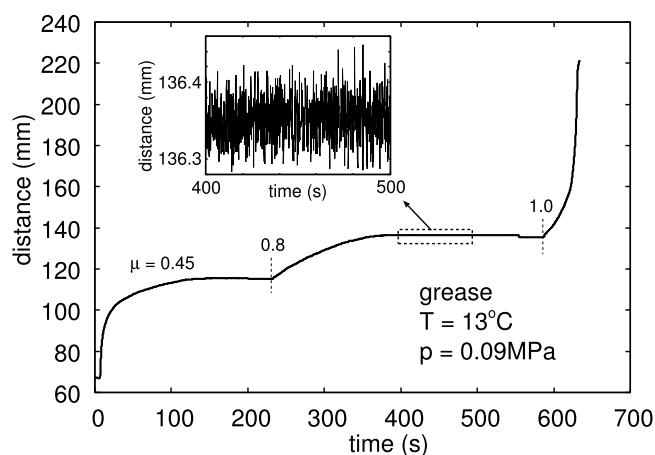

FIG. 6. Sliding dynamics for the interface lubricated by a grease when the driving force is increased in steps. The inset shows that in the stop-region, to within the accuracy of ∼0.01 mm, no slip occur.

μF_N (where $F_N = pA_0$ is the normal force) with $\mu = 0.45$. This results in a slip which finally stops after the sliding distance ≈ 50 mm. At this point, we increase the driving force to μF_N with $\mu = 0.8$. In this case too, the slip stops after sliding another ≈ 20 mm. Finally, we increase the driving force to $\mu = 1.0$. At this point, the slider accelerates until reaching the end of the sliding track, i.e., the sliding motion does not stop at this value of the driving force.

The inset in Fig. 6 shows that in the stop-region for $\mu = 0.8$, to within the accuracy of ~0.01 mm, no slip occurs during 100 s, so the slip velocity, if non-zero, must be below 10^{-7} m/s.

The result in Fig. 6 shows that in spite of the fact that after the first slip event with $\mu = 0.45$ it appears to the naked eye that all the grease is removed from the rubber-substrate contact region (see Fig. 3), the surface is still covered by a thin grease film. When increasing the driving force to $F_x = \mu F_N$ with $\mu = 0.8$, the sliding continues and further grease is removed (by the process shown in Fig. 4), until the grease film becomes so thin as to generate such high friction force that the motion stop.

Let us compare the results presented above with another case where glycerol is used as lubricant instead of the grease. Glycerol is a Newtonian fluid up to very high shear rates and therefore often used in model experiments.

Fig. 7 shows the sliding dynamics for the contact lubricated by glycerol, when the driving force is increased in steps. At time $t = 0$, the driving force is increased from zero to μF_N (where $F_N = pA_0$ is the normal force) with $\mu = 0.32$. This results in an initial rapid slip (about ~5 mm slip distance), during which most of the glycerol is removed (by the process shown in Fig. 4), followed by a period of very low velocity sliding. Next we increase the driving force to μF_N with $\mu = 0.43$. In this case too, very rapid slip occurs during ≈ 5 mm, followed by a second stage of very low velocity slip. This process repeats itself until we increase the driving force to $\mu = 0.76$. At this point, the slider accelerates until reaching the end of the sliding track, i.e., the sliding motion does not stop at this value of the driving force.

It is interesting to note that while for the grease covered surface the sliding motion stops after some short sliding distance, for the glycerol covered surface, low-velocity steady
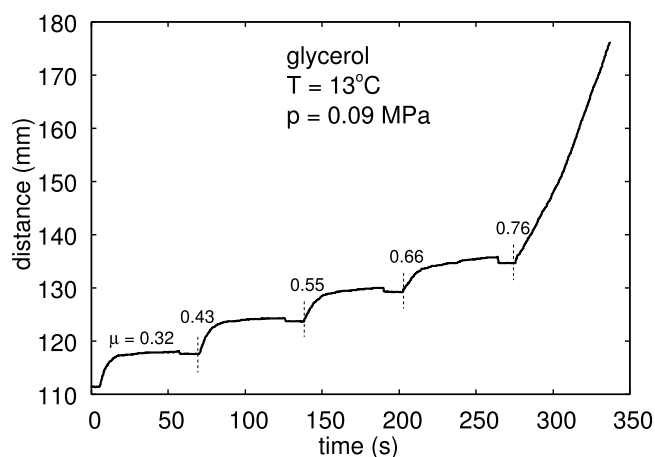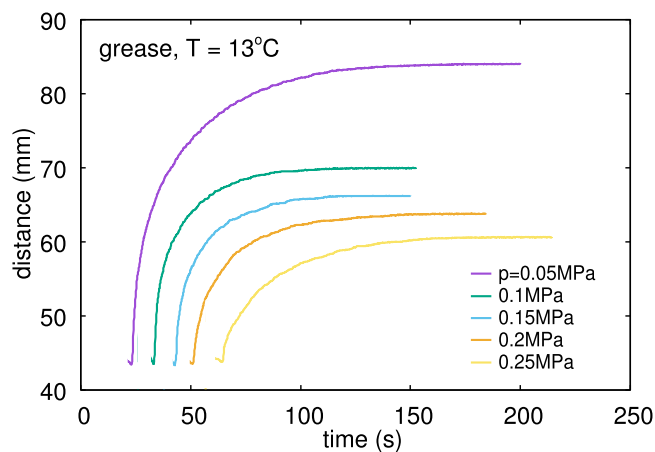
FIG. 8. The sliding distance as a function of time for the silicone rubber block sliding on the grease lubricated polymer substrate. Results are shown for the nominal contact pressures $p = 0.05$, 0.1, 0.15, 0.2, and 0.25 MPa. After the normal load was applied, one minute waiting time was used, before applying the driving force $F_x = 19$ N, which was the same in all cases.

sliding is observed in the second stage of the slip event. Assuming a uniform glycerol film thickness (e.g., neglecting the influence of the surface roughness), from the slip velocity v determined by the slope of the low-velocity steady sliding regions in Fig. 7 (giving v between 17 and 33 μm/s), one can determine the glycerol film thickness $d = \eta v/(p\mu) \approx 1$ nm, where we have used the glycerol viscosity $\eta = 2$ Pa s. Clearly, the surface roughness cannot be neglected in the study (calculations show that at the present nominal contact pressure $p = 0.09$ MPa, all the load is carried by the asperity contact regions already when the average surface separation is ≈ 100 nm).

Here it is interesting to note the much higher slip velocities are observed with PMMA. In this case, for the grease covered surface at $\mu = 0.18$, we observe steady sliding (close to the end of the sliding track) with a speed of about $v \approx 10$ cm/s. Assuming the shear viscosity $\eta = 10$ Pa s (as measured for the shear rate $v/d \approx 10^3$ s^{-1}), we get the surface separation $d = \eta v/(p\mu) \approx 0.1$ mm which is similar to the estimated (from the grease volume and surface area) thickness of the grease layer.

Fig. 8 shows the sliding distance as a function of time for the silicone rubber block sliding on the grease lubricated polymer substrate. Results are shown for several normal loads F_N, corresponding to the nominal contact pressures $p = 0.05$, 0.1, 0.15, 0.2, and 0.25 MPa. After the normal load was applied, one minute waiting time was used, before applying the driving force $F_x = 19$ N, which was the same in all cases. As expected, as the normal load increases, the slip distance before stop decreases.

IV. DISCUSSION

The results presented above have implications also for the sliding dynamics of soft bodies with shapes different from the rectangular shape. Thus, even when a (soft) spherical (or cylindrical) body is squeezed against a flat surface in a fluid, the center of the contact will bend upwards due to the fluid pressure, and the surface separation will have a local maximum

FIG. 7. Sliding dynamics for silicone rubber with the interface lubricated by a glycerol when the driving force is increased in steps.

at the center, as in Fig. 4 (see, e.g., Ref. 20). Hence, during sliding, similar effects as discussed above may take place. This could explain some surprising experimental observations we made in the past. For example, in Ref. 7, the breakloose friction force was studied as a function of the time of stationary contact when a rubber cylinder was squeezed against a flat countersurface in fluids. It was found that different fluids with very different viscosity gave very similar breakloose friction forces, and that, as a function of the time of stationary contact, the breakloose friction increased faster (towards a value close to that of the dry contact), than prediction from the theory assuming shearing the area of real contact formed during squeeze-out. Similarly, Roberts and Tabor[6] observed that the friction force calculated, assuming instantaneous shearing of the contact formed between soft solids in a fluid, will not give the observed breakloose friction force. These deviations between experimental observations and what is expected from theory may be related to transient elastohydrodynamic effects similar to those discussed in this paper.

The results presented above may be important in many applications involving friction and adhesion on lubricated or contaminated surfaces, e.g., for tires and shoes,[12–14] syringes, dynamic rubber seals, rubber belts used for generating traction on fluid contaminated surfaces, and for adhesion and friction in biological applications, e.g., between the tree frog toe pads and the countersurface. As an application, let us briefly discuss the tree frog adhesion problem.

Tree and torrent frogs can adhere and move on many types of surface, even during rain. Indeed, experiments have shown that, on a rotating platform flooded with water, the frogs toe pads will frequently slip on the smooth surface, reattaching after a small slide of at most a few centimeters.[15] Their toe pads are elastically very soft (4–20 kPa in Litoria caerulea[16]), so, during slips, the same fluid removal process as discussed above should prevail. Hence we believe that the slip will rapidly remove almost all of the fluid between the toe pads and the countersurface. On flooded surfaces, capillary adhesion is most likely absent, and the adhesion will be due to the viscosity of the fluid. Any tendency for the pads to detach from the surface will be resisted by a large negative pressure that develops in the thin fluid film under the pad, which therefore acts as a strong, hydrodynamic adhesive (viscous adhesion). In fact, we have observed the same effect in the experiments with the soft silicone rubber blocks: at the end of the slip on the (grease or glycerol) lubricated polymer surface, a very large force was necessary to remove the wood plate with the rubber blocks from the substrate. Often the pull-off force was so high as to break the glue-bond between the rubber blocks and the wood plate, i.e., the rubber blocks detached from the wood plate during pull-off.

The effect discussed above may also be important for the adhesion between the tree frog toe pads and a dry countersurface, which is believed to involve capillary bridges formed at the interface from fluid injected from the toe pad.[17,18] Strong (capillary or viscous) adhesion requires a very thin fluid film at the interface between the toe pad and the countersurface. When a tree frog lands on a surface after a jump, the impact force may be rather high (corresponding to contact pressure of order[19] ~30 kPa, i.e., similar to the Youngs

Wet adhesion in tree frogs

FIG. 9. Tree frog sliding after landing on a bamboo steam. Note the fluid film on the bamboo surface in the region where the toe pads were in contact with the bamboo surface. Courtesy of Jon Barnes research group.

modulus of the toe pad) and fluid may be squeezed out from the toe pad to the countersurface. If the fluid film is too thick, some slip may be necessary to reduce the fluid film thickness in order to generate high enough adhesion and friction. An illustration of this is shown in Fig. 9.

One fundamental problem we have not addressed in this work is how the dynamic scrape process depends on the width of the block in the sliding direction, and on the height of the block. This knowledge could be crucial for many applications, e.g., for the optimum design of the size of the rubber tread blocks in shoe soles. Thus for rubber blocks on a rigid backup (as the wood plate in the present study), if the height of the rubber blocks is much smaller than their width in the sliding direction, the upward bending of the bottom surface of the block will be reduced, resulting in a reduced scrape effect and smaller friction. This is consistent with friction studies[14] for shoe soles on (thin) water covered surfaces where the friction coefficient increased by ~0.1–0.2 when the groove depth was increased from 1 mm to 5 mm (in this case, part of the increase in the friction could also be due to the larger fluid flow channels which may result in faster transfer of the fluid to the outside of the sole foot print area). We plan to study how the dynamic scrape process depends on the height and width of the block in another publication. However, it is clear already from this study (see Fig. 2) that for rapid removal of fluid contamination (e.g., mud), and for the minimization of the slip distance, the tread blocks should be made from as soft rubber as possible.

V. SUMMARY AND CONCLUSION

We have performed simple, Leonardo da Vinci type, sliding friction experiments and observed a remarkable effect of scientific interest and practical importance: When a rectangular rubber block is slid on a flat lubricated substrate, the lubricant fluid is rapidly removed resulting in similar friction as for the dry interface. For elastically stiffer material, such as PMMA, we instead observed a monotonic increase in the

sliding speed (acceleration), and the lubricant film thickness appears to increase. We have explained the experimental observations qualitatively as a transient elastohydrodynamic effect, which we refer to as the dynamic scrape mechanism. The results presented above may be important, e.g., for the movement of objects along lubricated or contaminated surfaces, e.g., for tires, dynamic seals, or syringes.[7]

ACKNOWLEDGMENTS

APPENDIX A: MATERIAL PROPERTIES

In this appendix, we present information about the surface topography and material properties for the materials involved in the study above. We first show the surface roughness power spectra of the powersil silicone rubber and polymer substrate surfaces. Next we study the viscoelastic properties of the silicone rubber and present some results for the rheology properties of the grease.

1. Surface roughness power spectra

Using an engineering stylus instrument and Atomic Force Microscopy (AFM) we have measured the surface topography of the silicone rubber and polymer surfaces used in our friction study. From the measured data, we calculated the surface roughness power spectra.
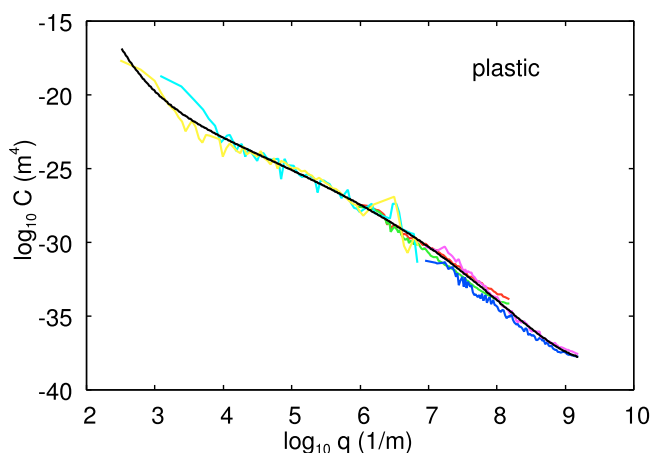

FIG. 10. The 2D surface roughness power spectrum C as a function of the wavenumber q ($\log_{10}$–$\log_{10}$ scale) for the red polymer surface. The topography was measured using engineering line-scan (curves for the lower wavenumbers) and Atomic Force Microscopy (AFM) (curves for the larger wavenumbers). In the calculation, we use the black fit-curve.

Figs. 10 and 11 show the 2D surface roughness power spectrum $C(q)$ as a function of the wavenumber q ($\log_{10}$–$\log_{10}$ scale) for the red polymer surface and the powersil rubber surface, respectively. The black lines are fit-curves.
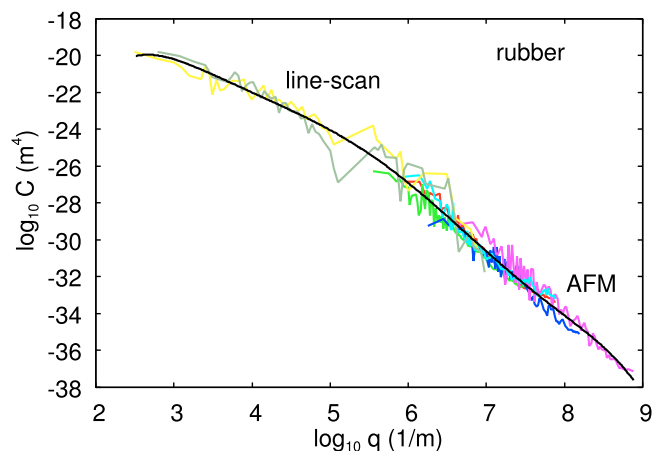

FIG. 11. The 2D surface roughness power spectrum C as a function of the wavenumber q ($\log_{10}$–$\log_{10}$ scale) for the powersil silicone rubber surface. The topography was measured using engineering line-scan (curves for the lower wavenumbers) and Atomic Force Microscopy (AFM) (curves for the larger wavenumbers). In the calculation, we use the black fit-curve.

FIG. 12. The 2D surface roughness power spectrum fit curves (from Figs. 10 and 11) as a function of the wavenumber q ($\log_{10}$–$\log_{10}$ scale) for the red polymer and rubber surfaces.

FIG. 13. The height probability distribution for all the red polymer and silicone rubber surfaces used in this study.
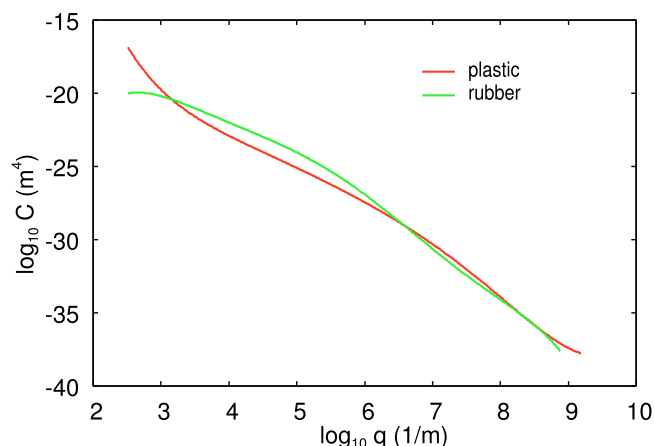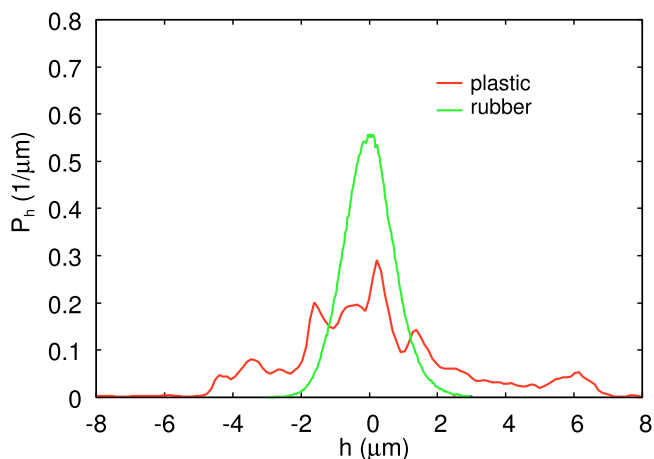
Fig. 12 shows the 2D surface roughness power spectrum fit curves (from Figs. 10 and 11) as a function of the wavenumber q ($\log_{10}$–$\log_{10}$ scale) for the red polymer and powersil rubber surfaces.

In the calculations below, we use the two power spectra given by the black lines in Figs. 10 and 11. The largest wavenumber is of order $q_1 \approx 10^9$ m (corresponding to a roughness wavelength $\lambda = 2\pi/q \approx 6$ nm).

The distribution of surface heights for the studied surfaces is shown in Fig. 13. Note that the root-mean-square (rms) roughness of the surfaces is of order ~1 μm. The rms roughness depends mainly on the longest wavelength roughness components and will therefore also depend on the length of the line scan (in this case of order cm).

Rubber viscoelastic modulus

We have measured the viscoelastic modulus of the rubber compounds using Dynamic Mechanical Analysis (DMA) in oscillatory elongation mode. The measurements are performed at many different temperatures (namely 40), and within a fixed frequency interval. The temperature segments are shifted along the frequency axis in order to obtain the viscoelastic master curve $E(\omega, T_{\text{ref}})$ (at a given reference temperature T_{ref}), and the shift factor a_T. The viscoelastic modulus at any temperature and frequency is obtained as $E(\omega, T) = E(\omega a_T, T_{\text{ref}})$.

The red curve in Fig. 14 shows the viscoelastic modulus master curve for the powersil rubber compound resulting from shifting ReE. Also shown is the viscoelastic modulus of a standard polydimethylsiloxane (PDMS) rubber compound (green curve), Sylgard 184, which has been used in many model studies of rubber contact mechanics and friction. We have used the reference temperature $T_{\text{ref}} = 20\,°C$ and the dynamic strain amplitude 0.04%.

Note the abrupt increase in the powersil modulus for the frequency $f = f_c \approx 10^5$ Hz. This is due to freezing (crystallization) of the rubber, implying that (for temperatures above the freezing temperature) the viscoelastic data in Fig. 14 cannot be trusted in the frequency region $f > f_c$. Fortunately, for the sliding speeds most relevant for the applications, the frequency region $f < f_c$ is most important.

Fig. 15 shows the shift factor a_T for the powersil rubber compound (red curve) and of Sylgard 184 silicon rubber compound (green curve). The figure shows that the freezing (crystallization) occurs for the temperature $T \approx -60\,°C$.

Rheology of the grease

The effective viscosity η of the grease used in the friction experiments is shown in Fig. 16 at the temperature $T = 25\,°C$. Note that the viscosity increases as the shear rate decreases, i.e., the grease exhibits shear thinning. For the shear rate
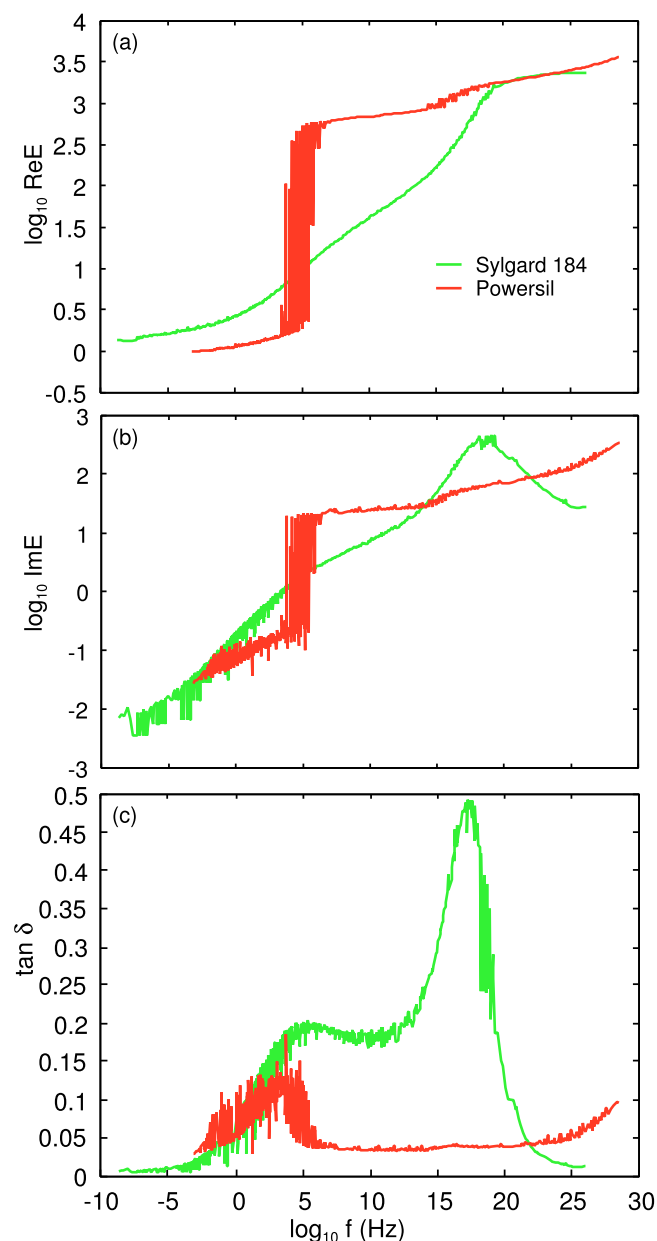

FIG. 14. The viscoelastic modulus master curves for the powersil rubber compound (red curve) and of Sylgard 184 silicon rubber compound (green curve), resulting from shifting ReE. The reference temperature $T_{\text{ref}} = 20\,°C$ and the dynamic strain amplitude is 0.04%.
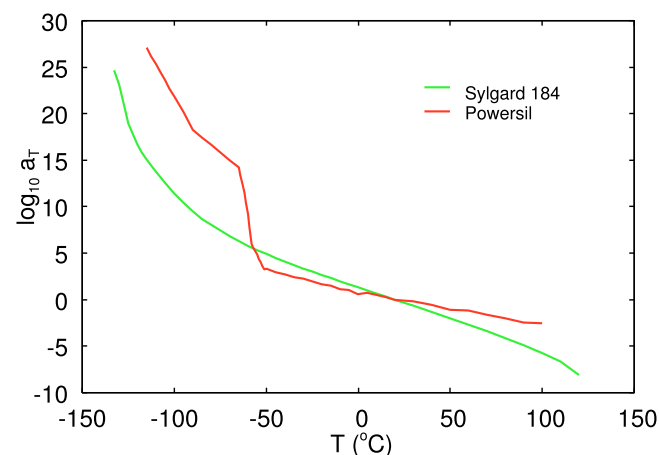

FIG. 15. The shift factor a_T for the powersil rubber compound (red curve) and of Sylgard 184 silicon rubber compound (green curve), resulting from shifting ReE. We believe the abrupt increase in a_T (read curve) when the temperature decreases below $T \approx -60\,°C$ is due to crystallization of the powersil rubber compound.
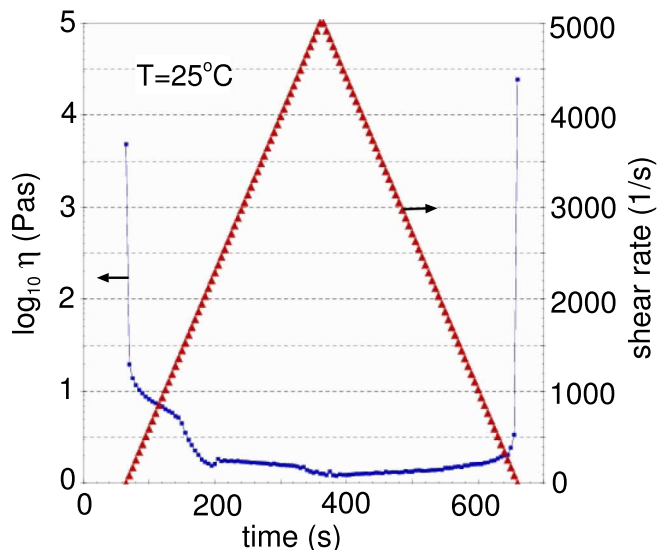
FIG. 16. The logarithm of the effective viscosity η (defined as shear stress τ divided by the shear rate $\dot{\gamma}$) as a function of time during strain rate cycling. The strain rate increases linear with time to a maximum $\dot{\gamma} = 5000$ s^{-1}, and then decreases linearly with time to zero. The temperature $T = 25$ °C. Courtesy of Klüber lubrication Deutschland.

$\dot{\gamma} \approx 1000$ s^{-1}, the effective viscosity $\eta \approx 10$ Pa s. Extrapolation of the shear stress $\eta\dot{\gamma}$ to zero shear rate gives a yield stress of order 1 kPa.

APPENDIX B: SQUEEZE-OUT AND DEWETTING

In this appendix, we first study the influence of the surface roughness on the fluid squeeze-out assuming no sliding and no dewetting. We also discuss dewetting of asperity contact regions, i.e., local dewetting at short length scales.

In Sec. III, we showed that in the present context, assuming perfectly smooth surfaces and neglecting the deformations of the rubber surface by the fluid pressure (which would slow down the fluid squeeze-out), it takes ~33 yr to squeeze-out the fluid (glycerol) down to a thickness of order ~1 nm. Here we show that including the (measured) surface roughness will shorten the squeeze-out time by a factor ~10^3 (from ~10^9 s to ~10^6 s). However, this fluid squeeze-out time is still much longer than the time ~10 s needed to reduce the film thickness to ~1 nm during slip (see Sec. III and Figs. 7 and 18).

The surface roughness influences the fluid flow via the fluid pressure flow factor ϕ, which is a function of the average interfacial surface separation $\bar{u}$. The flow factor ϕ enters the fluid flow equation together with the fluid viscosity η in the combination $\eta_{\text{eff}} = \eta/\phi(\bar{u})$. For surfaces with isotropic roughness, $\phi(\bar{u}) < 1$, which correspond to an effective viscosity $\eta_{\text{eff}} > \eta$. Thus, for a given average interfacial separation, the surface roughness slows down the fluid removal (see Fig. 17). However, when roughness exists, the average surface separation is non-zero also when all fluid is squeezed out from the asperity contact regions, and calculations show that fluid squeeze-out, down to the point where the total load is carried by dry asperity contact regions, occurs faster when the surface
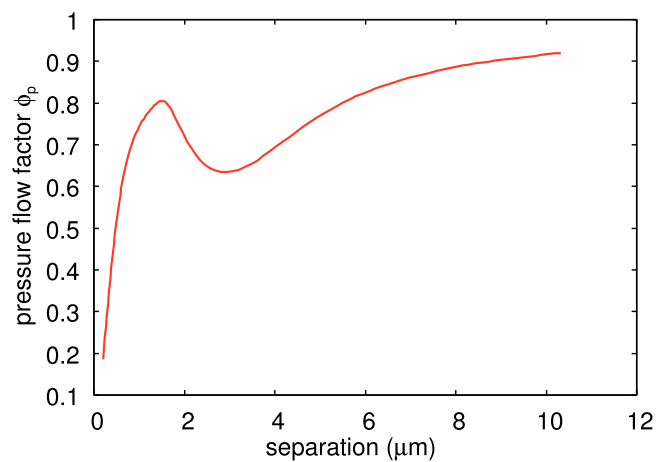

FIG. 17. The pressure flow factor calculated using the surface roughness power spectrum obtained from the measured surface roughness profiles of the rubber and the polymer substrate.

roughness amplitude increases. This is due to the non-contact fluid flow channels, which prevail in the apparent contact region, which allow the fluid to be channeled to the outside of the nominal contact area.[21]

The fluid pressure flow factor can be calculated approximately using the Bruggeman effective medium theory,

$$\frac{1}{\phi} = \frac{A}{A_0}\frac{2}{\phi} + \int du\, P(u)\frac{2}{\phi + (u/\bar{u})^3},$$

where $P(u)$ is the distribution of interfacial separation (which we calculate using the equations derived in Ref. 22), and where $\bar{u}$ is the average interfacial separation. The relative contact area A/A_0 and $\bar{u}$ both depend on the ratio p/E between the nominal contact pressure and the Young's modulus and are calculated as described in Ref. 23. Thus, the flow factor depends on the surface roughness power spectrum and on p/E or, alternatively, on $\bar{u}$. Fig. 17 shows the pressure flow factor as a function of $\bar{u}$ calculated using the surface roughness power spectrum obtained from the measured surface roughness profiles of the rubber and the polymer substrate (see Appendix A).

Fig. 18 shows the calculated surface separation (a), and the contact area (b), as a function of time. The (low frequency) Young's elastic modulus $E = 1.5$ MPa was obtained from DMA measurements, and the nominal contact pressure $p = 0.09$ MPa. The result for other viscosities can be obtained by scaling the time-axis (the squeeze-out depends on t/η). Note that for time $t > 10^6$ s, both the average interracial separation and the contact area become time independent. Thus, it takes $t = 10^6$ s to removed the fluid completely from the asperity contact regions; at this point in time all the load is carried by the dry asperity contacts.

We now discuss the role of dewetting. A fluid between two solid walls can be removed spontaneously if the interfacial free energy is lowered when forming the dry contact. For perfectly flat surfaces (no surface roughness), this is the case if the spreading pressure $S = \gamma_{S_0S_1} - \gamma_{S_0L} - \gamma_{S_1L}$ is negative. Here $\gamma_{S_0S_1}$ is the interfacial free energy between solid S_0 and S_1, and γ_{S_0L} is the interfacial energy between solid S_0 and the liquid L, and similar for γ_{S_1L}. If $S > 0$, the liquid likes to stay
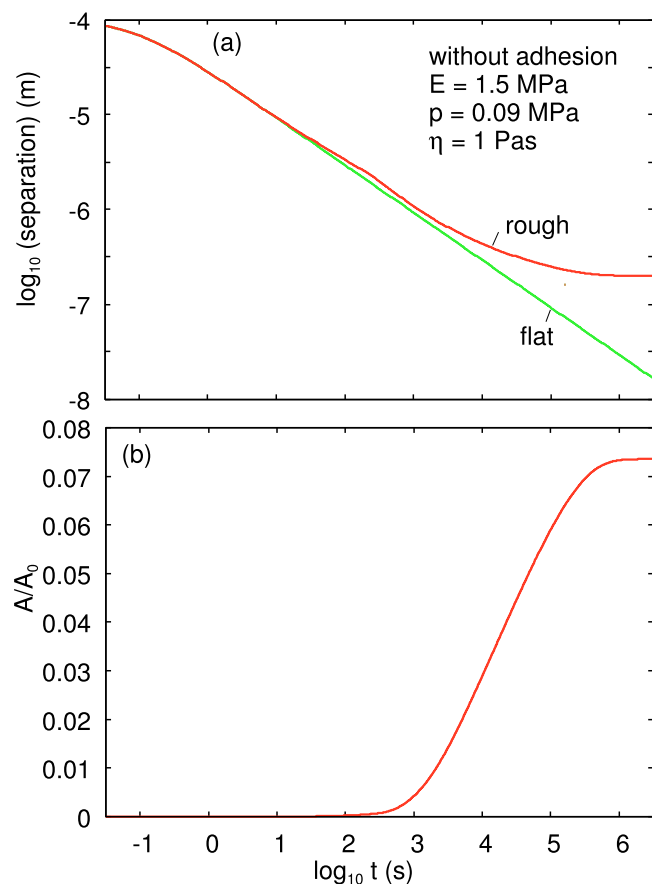
FIG. 18. The surface separation (a) and the contact area (b) as a function of time. The Young's elastic modulus $E = 1.5$ MPa, the nominal contact pressure $p = 0.09$ MPa and the fluid viscosity $\eta = 1$ Pa s. The result for other viscosities can be obtained by scaling the time-axis (the squeeze-out depends on t/η). The surface roughness power spectrum was obtained from the measured surface roughness profiles of the rubber and the polymer substrate. The rectangular rubber block is $L_x = 1.25$ cm long in the fluid flow direction.

between the surfaces (it acts like a lubricant) and is removed only if a large enough external pressure acts at the interface. If $S < 0$, the fluid film is unstable and the asperity contact regions dewet resulting in dry contact regions. In this case, an effective (short-ranged) attractive interaction occurs between the surfaces, and $-S$ is the work to separate the surfaces in the fluid, i.e., the work of adhesion in the fluid.

Global dewetting typically nucleates at the point where asperity contact first occurs, and then spreads laterally with a speed which depends on the fluid viscosity and the rubber viscoelastic modulus.

We cannot exclude that in some cases in Sec. III, dewetting may influence the fluid film thickness during the last stage of fluid removal, where asperity contact occurs between the surfaces. However, we have observed the same effect as discussed in this paper (dynamic scrape) also in other cases where dewetting does not take place, e.g., for a hydrocarbon oil on a steel surface (which is wetted by the oil), in contact with non-silicon rubber block.

We note that if global fluid removal would occur via dewetting, one would expect much faster fluid removal from the contact interface than we observe. Thus, even for the silicon rubber and glycerol system, the fluid is not removed
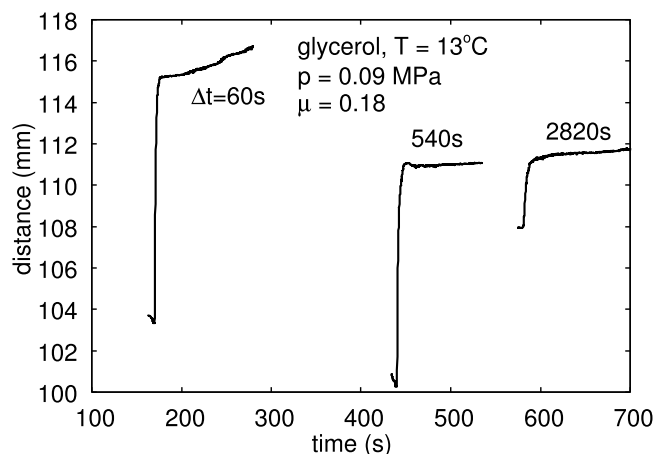

FIG. 19. Sliding dynamics for the interface lubricated by a glycerol. The sliding distance is shown as a function of the time, after three different times Δt of stationary contact.

after a relative long squeezing time (about 1 h) (see Fig. 19). In this case, the film thickness is reduced due to squeezing, and Fig. 18 shows that some asperity contact occur, but the high initial sliding speed which is observed, even when a small driving force is applied (see Fig. 19), shows that there is still a fluid film between most of the surfaces. Thus, only sliding is able to rapidly remove the fluid film, resulting in a complete stop of slip (for the grease), or followed by a second stage of slip at a very low sliding speed as observed for the glycerol lubricated interface.

Let us discuss dewetting in more detail. We first show, in accordance with the discussion above, that global dewetting is unlikely to occur. Next we show that, at least for glycerol, local dewetting may take place in some asperity contact regions, see Fig. 20. We note that global dewetting, and local dewetting, would result in nearly the same (low speed) sliding friction. However, the fluid squeeze-out time could differ dramatically for these two cases. Global dewetting starts (nucleate) when the first contact occur between the two surfaces (involving the highest asperities), and then spread rapidly resulting in fast dewetting. On the other hand, local dewetting may occur at each asperity contact area independent of the status of the other contact regions. In this case, fluid removal from the interface is mainly due to the applied normal force and is usually a very slow process.
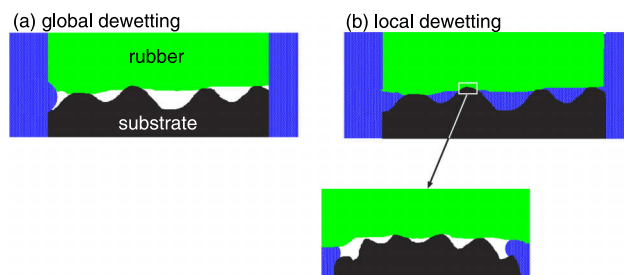

FIG. 20. Rubber block (green) squeezed against a rough substrate (black) in a fluid (blue). After long enough time the fluid will wet the whole interface (not shown), or else (a) be completely removed from the interface (global dewetting) or (b) only from some asperity contact regions (local dewetting).

Using the Young's equation, one can write

$$S = -w + \gamma(\cos\theta_0 + \cos\theta_1), \qquad (B1)$$

where θ_0 and θ_1 are the fluid contact angles on solid S_0 and S_1, respectively, and where γ is the fluid surface tension and w the work of adhesion to separate the solid surfaces without the fluid. We assume that (B1) is valid also for surfaces with roughness. Using the language of the renormalization group theory, one obtains w, θ_0, and θ_1 to be used in (B1) by integrating out the roughness with wavelength shorter than the length scale under consideration. Thus the work of adhesion w, and the contact angles θ_0 and θ_1, depends on the surface roughness. In addition, contact hysteresis occur, and the gain in free energy during contact formation is smaller than the energy needed for separation (this is due, e.g., to elastic instabilities occurring during separation). Similarly the contact angles θ_0 and θ_1 depend on if the fluid is advancing or receding on the surface. For the dewetting, it is clear that what matters is the work of adhesion during contact formation and the contact angles θ_0 and θ_1 for a receding contact line.[24,25] For our systems, calculations (see Fig. 21) show that (because of the surface roughness) the work of adhesion on contact formation vanishes. For glycerol we measured the advancing and receding contact angles on the silicone rubber to be $\approx 95°$ and $45°$, respectively, and on the polymer (substrate) surface $\approx 85°$ and $35°$, respectively.[26] Using the receding contact angles gives $(\cos\theta_0 + \cos\theta_1) \approx 1.6$. The glycerol surface energy is $\gamma \approx 0.06$ J/m^2. Thus we get $S \approx -0.0 + 0.06 \times 1.6 > 0$ and we conclude that most likely no *global* dewetting takes place for the silicone rubber — glycerol — polymer interface.

Let us now apply (B1) on a local scale, to study if dewetting occurs in the macroasperity contact regions, or at smaller length scales in the asperity contact regions [see
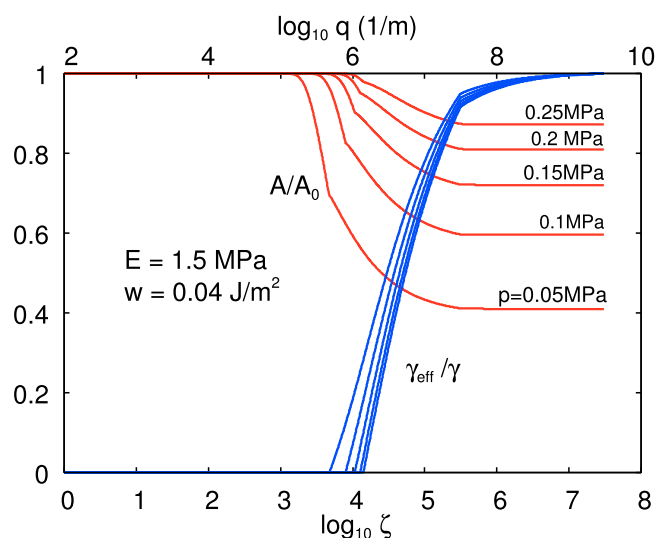

FIG. 21. The relative contact area (red lines) and the normalized effective interfacial energy $\gamma_{\mathrm{eff}}/\gamma$ (where γ is the free energy per unit surface for surfaces without roughness) (blue lines), as a function of the logarithm of the magnification. Results are for the contact pressures $p = 0.05$, 0.1, 0.15, 0.2, and 0.25 MPa. Calculated results using the Young's elastic modulus $E = 1.5$ MPa and the work of adhesion $w = 0.04$ J/m^2, and the surface roughness power spectrum obtained from the measured surface roughness profiles of the rubber and the polymer substrate.

Fig. 20(b)]. First note that the silicone rubber we use (powersil 600 A/B) is intrinsically a heterogeneous polymer with siliceous fillers.[27] Even though the filler is partially modified by organic groups, it imparts non-negligible polarity of the polymer as evidenced from the high contact angle hysteresis. For water on PDMS rubber, the hysteresis is $20°$–$40°$, as compared to $\sim 5°$ on a pure PDMS matrix. Most likely the filler particles is also the origin of the inhomogeneous (non-random) distribution of surface charges observed (using Kelvin Force Microscopy maps of the surface electrostatic potential) in Ref. 28 after separating a PDMS sheet in adhesive contact with another PDMS sheet. The analysis of the data in Refs. 29 and 30 indicated a charge-charge correlation length, which we interpret as the average patch size, of order 0.1–1 μm. We note that practically all types of rubber used in industrial applications contain fillers. Hence large contact hysteresis (at the macroscopic length scale) for polar liquids may be very common, and may be very important for the dewetting dynamics. Thus, in a polar liquid (e.g., water) at the micrometer (and smaller) length scales, patches of dry and wet areas may prevail, which could strongly influence the contribution to the friction from the area of contact.

We have argued above that global dewetting cannot occur. Let us now study the (apparent) asperity contact regions as we increase the magnification. Fig. 21 shows that when the magnification $\zeta > 10^4$, corresponding to the length scale or resolution $1/q = 1/(\zeta q_0) < 1$ μm, the work of adhesion $\gamma_{\mathrm{eff}}(\zeta)$ is non-zero (the results in the figure is calculated using the theory presented in Ref. 31). Furthermore, at short enough length scale (of order 0.1–1 μm), we likely will observe patches of hydrophobic and hydrophilic silicone rubber, where the local fluid (glycerol) contact angle may be similar to the advancing and receding contact angles observed at the macroscopic length scale. Assuming the same is true for the substrate, there may be regions on the surface where the local contact angle is of order $90°$ on both surfaces (see above) in which case $\cos\theta_0 + \cos\theta_1$ will be close to zero. Since the local work of adhesion γ_{eff} approaches the value expected for smooth surfaces as the magnification increases, $\gamma_{\mathrm{eff}}(\zeta) \approx \gamma \approx 0.05$ J/m^2, it is clear that locally $S(\zeta)$ may be negative, for large enough ζ. Thus, even if no global dewetting occur, it is still possible that the fluid is expelled locally from many asperity contact regions observed at high magnification, see Fig. 20. Thus the friction coefficient when the interface is "lubricated" by glycerol (or by water) may after a long enough time exhibit a friction resulting from shearing an area of real contact which has some dry contact regions and some wet (lubricated) contact regions. This however, does not reduce the importance of the dynamical scraping mechanism in removing most of the fluid and facilitating asperity contact between the solids.

In this context, we note that Dhinojwala and coworkers[32] have studied sliding friction and adhesion for PDMS against sapphire. They found that in water, the friction coefficient was about half of the friction coefficient for the dry interface. Using sum-frequency generation spectroscopy, they were able to show that some fraction of the interface was dry (but with one monolayers of water molecules adsorbed on the sapphire surface), while in the other fraction of the interface, the surfaces were separated by thin water film. As discussed

above, this granular or patchy dry-wet state of the interface could be related to hydrophobic and hydrophilic regions on the silicone rubber surface.

[1] A. C. Dunn, J. A. Tichy, J. M. Uruena, and W. G. Sawyer, Tribol. Int. **63**, 45 (2013).

[2] W. B. Dapp, A. Lucke, B. N. J. Persson, and M. H. Müser, Phys. Rev. Lett. **108**, 244301 (2012).

[3] D. Dowson and G. R. Higginson, J. Mech. Eng. Sci. **1**, 6 (1959).

[4] R. Gohar, *Elastohydrodynamics*, 2nd ed. (World Scientific Publishing, Singapore, 2001).

[5] B. N. J. Persson and M. Scaraggi, Eur. J. Phys. E **34**, 113 (2011).

[6] A. D. Roberts and D. Tabor, Proc. R. Soc. A **325**, 323 (1971).

[7] B. Lorenz, B. A. Krick, N. Rodriguez, W. G. Sawyer, P. Mangiagalli, and B. N. J. Persson, J. Phys.: Condens. Matter **25**, 445013 (2013).

[8] B. Lorenz, Y. R. Oh, S. K. Nam, S. H. Jeon, and B. N. J. Persson, J. Chem. Phys. **142**, 194701 (2015).

[9] In the study below, we added the loading mass not at the center of the wood plate, but slightly behind the midpoint of the block. In this case, there will be slightly larger normal force acting on the (rubber or PMMA) block located at the trailing edge than at the block at the leading edge. Thus, the wood plate will slightly tilt in such away as to facilitate the build-up of hydrodynamic pressure in the fluid film during slip. This is probably the reason for why for PMMA the fluid film thickness appears to increase during slip. However, in spite of this loading-induced tendency to generate a fluid film pressure build-up during slip, for the soft rubber blocks, the fluid is removed after a short sliding distance.

[10] B. N. J. Persson, *Sliding Friction: Physical Principles and Applications* (Springer, Heidelberg, 2000).

[11] E. Gnecco and E. Meyer, *Elements of Friction Theory and Nanotribology* (Cambridge University Press, 2015).

[12] T. K. Courtney, S. K. Verma, W.-R. Chang, Y.-H. Huang, D. A. Lombardi, M. J. Brenner, and M. J. Perry, Occup. Environ. Med. **70**, 35 (2013).

[13] W.-R. Chang, Appl. Ergonomics **32**, 173 (2001).

[14] K. W. Li, H. H. Wu, and Y.-C. Lin, Appl. Ergonomics **37**, 743 (2006).

[15] T. Endlein, W. J. P. Barnes, D. S. Samuel, N. A. Crawford, E. A. Btaw, and U. Grafe, PLoS ONE **8**, e73810 (2013).

[16] W. J. P. Barnes, P. J. P. Goodwyn, M. Nokhbatolfoghahai, and S. N. Gorb, J. Comp. Physiol., A **197**, 969 (2011).

[17] W. Federle, W. J. P. Barnes, W. Baumgartner, P. Drechsler, and J. M. Smith, J. R. Soc., Interface **3**, 689 (2006).

[18] B. N. J. Persson, J. Phys.: Condens. Matter **19**, 376110 (2007).

[19] M. Kappl, F. Kaveh, and W. J. P. Barnes, "Nanoscale friction and adhesion of tree frog toe pads," Bioinspir. Biomim. (in press).

[20] M. Scaraggi and B. N. J. Persson, Tribol. Lett. **47**, 409 (2012).

[21] B. Lorenz and B. N. J. Persson, Eur. Phys. J. E **32**, 281 (2010). See also Ref. 2.

[22] A. Almqvist, C. Campana, N. Prodanov, and B. N. J. Persson, J. Mech. Phys. Solids **59**, 2355-2369 (2011).

[23] B. N. J. Persson, J. Chem. Phys. **115**, 3840 (2001).

[24] M. K. Chaudhury and G. M. Whitesides, Langmuir **7**, 1013 (1991).

[25] It has observed that using the receding contact angle gives results in good agreement with dewetting experiments even when the advancing angle is very large and receding angle is very low (M. K. Chaudhury, private communication (2016)).

[26] The hysteresis of hydrogen bonding polar liquids, such as water or glycerol, against silicone rubber is mainly due to hydrophilic patches on the rubber surface, resulting from the silica filler particles. This chemical heterogeneity of the rubber surface has usually a much stronger effect on the contact angle than the surface roughness (M. K. Chaudhury, private communication (2016)).

[27] K. H. Kim and M. K. Chaudhury, J. Adhes. **85**, 792 (2009).

[28] H. T. Baytekin, A. Z. Patashinski, M. Branicki, B. Baytekin, S. Soh, and B. A. Grzybowski, Science **333**, 308 (2011).

[29] B. N. J. Persson, M. Scaraggi, A. I. Volokitin, and M. K. Chaudhury, EPL **103**, 36003 (2013).

[30] K. Brormann, K. Burger, A. Jagota, and R. Bennewitz, J. Adhes. **88**, 589 (2012).

[31] B. N. J. Persson, Eur. Phys. J. E **8**, 385-401 (2002).

[32] K. Nanjundiah, P. Y. Hsu, and A. Dhinojwala, J. Chem. Phys. **130**, 024702 (2009).